

Enhancement of dielectric constant of BaTiO₃ nanoparticles studied by resonant x-ray emission spectroscopy

Nobuo Nakajima,* Megumi Oki, Yoichi Isohama, and Hiroshi Maruyama

Graduate School of Science, Hiroshima University, 1-3-1 Kagamiyama, Higashi-Hiroshima 739-8526, Japan

Yasuhisa Tezuka

Faculty of Science and Technology, Hirosaki University, 3 Bunkyo, Hirosaki 036-8561, Japan

Kotaro Ishiji

SAGA Light Source, 8-7 Yayoigaoka, Tosu, Saga 841-0005, Japan

Toshiaki Iwazumi

Graduate School of Engineering, Osaka Prefecture University, 1-1 Gakuen, Sakai, Osaka 599-8531, Japan

Kozo Okada

Graduate School of Natural Science and Technology, 3-1-1 Tsushima-naka, Okayama 700-8530, Japan

(Received 29 February 2012; revised manuscript received 6 November 2012; published 28 December 2012)

The nanoscopic origin of the enhancement of the dielectric constant of BaTiO₃ nanoparticles was investigated by means of Ti K β resonant x-ray emission spectroscopy. Two inelastic peaks due to charge-transfer excitations were observed, one of which disappeared as the particle size (d) was reduced, while the other remained unchanged. This is consistent with the fact that tetragonality was also reduced with decreasing d . The origin of the large enhancement in the dielectric constant is briefly discussed from a microscopic point of view.

DOI: [10.1103/PhysRevB.86.224114](https://doi.org/10.1103/PhysRevB.86.224114)

PACS number(s): 73.22.-f, 78.70.En, 77.80.-e

I. INTRODUCTION

Ferroelectric BaTiO₃ (BTO) particles are a key material in various applications, such as multilayered ceramic capacitors, infrared detectors, and positive temperature coefficient thermistors.¹⁻³ Due to strong demands on memory devices for downsizing and high-density recording, the required particle size (d) continues to rapidly decrease. With decreasing d , however, the crystal structure changes from tetragonal to cubic followed by an undesired decrease in ferroelectricity. Recently, a very large enhancement of the dielectric constant was observed at $d = 70$ nm,⁴ although the change in crystal structure from $d = 430$ nm (tetragonal) to 40 nm (cubic) is monotonic.⁵ The latter can be simply explained by a core-shell model proposed by Aoyagi *et al.*,⁶ which indicates that the volume fraction of a cubic shell gradually exceeds that of a tetragonal core with decreasing d . Still, this model is too simple to explain the enhancement in the dielectric constant for smaller d .

BTO is a typical displacive-type ferroelectric material; its ferroelectricity is the result of the positioning of Ti⁴⁺ ions at off-center sites in oxygen octahedra. Zalar *et al.* argued, using the results of an NMR study, that Ti displacement occurred even in the high-temperature cubic phase in a pure BTO single crystal.⁷ Similar Ti displacement is expected in cubic BTO nanoparticles. Very recently, a speckle experiment using a pulsed soft x-ray laser revealed spatial and temporal fluctuations of polarization clusters, and it was observed that their relaxation time has a maximum value at a temperature of 4.5 K above the Curie temperature (T_C) of 120 °C.^{8,9} Such fluctuations become important in the microscopic regime.

In our recent studies on bulk BTO,^{10,11} we have demonstrated that resonant x-ray emission spectroscopy (RXES)

is a suitable technique for detecting changes in the local bonding of an absorbing atom, especially in the case of the Raman process, wherein a coherent second-order process is described by the Kramers-Heisenberg formula. At the Ti K-edge excitation energy, two weak Raman peaks due to charge transfer (CT) excitations are observed in the Ti K β RXES spectra. One of the CT peaks shows a clear dependence on both temperature and applied electric field. The essential factor in these dependencies is the electric dipole moment produced by an off-center Ti in an oxygen octahedron, in other words, atomic scale polarization. Hence, RXES is suitable for detecting the physical and electronic properties of nanosized particles, in contrast to other conventional techniques, which reflect averaged and macroscopic properties.

In the present study, Ti K β RXES spectra of BTO nanoparticles were measured to investigate the origin of the enhancement of the dielectric constant. The particle size dependence of the Raman peaks was examined together with the tetragonality (c/a ratio) revealed by x-ray diffraction. A simple theoretical explanation based on the configuration interaction (CI) is proposed.

II. EXPERIMENTAL

Eight samples of BTO nanoparticles with average d of 20, 30, 50, 70, 85, 100, 120, and 200 nm were obtained from Toda Kogyo Corp. A hydrothermal method [Ba(OH)₂ + TiO₂ → BaTiO₃ + H₂O] was adopted to prepare the nanoparticles, instead of the conventional solid-phase method (BaCO₃ + TiO₂ → BaTiO₃ + CO₂). The structural properties were characterized by x-ray diffraction (XRD, Cu K α , Rigaku RINT-2000).

Ti $K\beta$ RXES measurements were carried out on the bending magnet beamline BL-7C at the Photon Factory of the High Energy Accelerator Research Organization (KEK-PF). The synchrotron radiation was monochromatized by a double-crystal Si(111) monochromator. X-ray absorption spectra (XAS) were measured by a transmission method using powder samples spread over adhesive tapes. The RXES spectra were obtained using a curved Ge(111) crystal monochromator installed in a vacuum chamber. The analyzed x-rays were detected by a position-sensitive proportional counter using a charge division method.¹² The overall experimental energy resolution was about 1 eV.

III. RESULTS

Figure 1(a) shows a transmission electron microscopy (TEM) image of BTO nanoparticles with $d = 100$ nm. Fine uniform particles were obtained by the hydrothermal method described above. All of the samples had a tetragonal structure with a space group $P4mm$ at room temperature [Fig. 1(b)]. The largest particles, with $d = 200$ nm, had a tetragonal structure with a c/a ratio almost identical to the bulk value. The XRD pattern shown in Fig. 1(c) demonstrates that the samples with $d < 100$ nm have greatly reduced tetragonality; i.e., the c/a ratio approaches unity with decreasing d . The shift of the $\{200\}$ peaks toward lower angle as d decreases from 85 to 20 nm reflects lattice relaxation accompanied by nanoscale crystallization. An additional point to be noted is that the change in linewidth for $d \leq 85$ nm is nonmonotonic. Single-peak Gaussian fits for $d \leq 85$ nm are displayed in Fig. 2(c) with their full-width-at-half-maximum (FWHM) values on the right. Broader peaks for $d = 70$ and 85 nm are indicative of a mixture of tetragonal and pseudocubic phases, even just below the abrupt decrease in tetragonality.

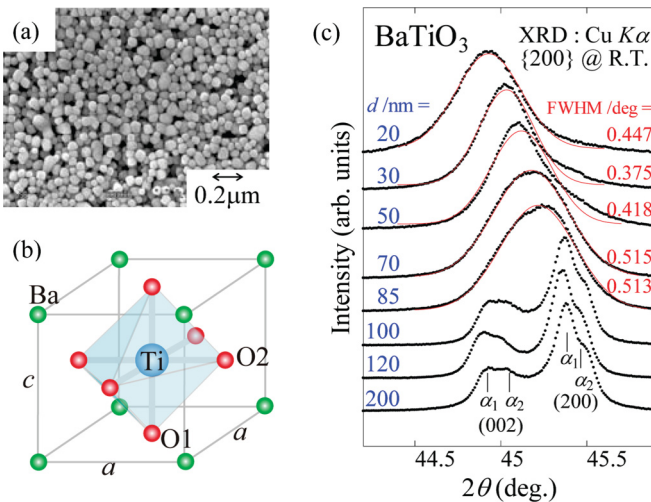


FIG. 1. (Color online) (a) TEM image of BaTiO₃ nanoparticles with $d = 100$ nm. (b) Crystal structure of BaTiO₃. Two nonequivalent oxygen sites, O(1) and O(2), exist in a ferroelectric phase. (c) X-ray diffraction patterns around the $\{200\}$ peaks for various d values measured at room temperature. The red (thin solid) lines for $d \leq 85$ nm are single-peak Gaussian fits with their full-width-at-half-maximum (FWHM) shown on the right.

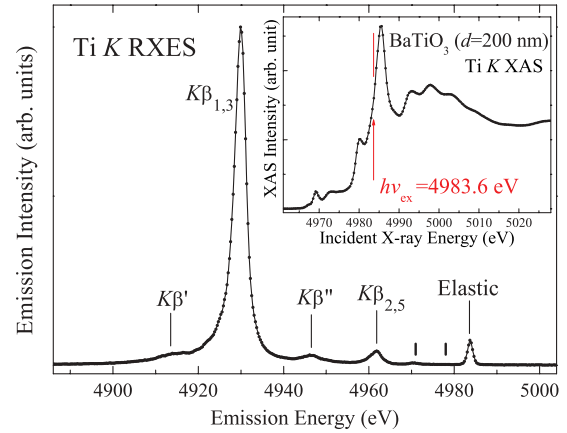


FIG. 2. (Color online) Ti $K\beta$ RXES spectrum of BTO nanoparticles with $d = 200$ nm at room temperature. The elastic peak corresponds to an excitation x-ray energy of 4983.6 eV, 1.7 eV below the white line in the XAS spectrum, as shown by the tick mark in the inset. Two tick marks with no assignment indicate the positions of Raman peaks due to charge transfer excitations.

Figure 2 shows the Ti $K\beta$ RXES spectrum of BTO nanoparticles with $d = 200$ nm. The excitation x-ray energy ($h\nu_{ex}$) was tuned to 4983.6 eV, 1.7 eV below the white line in the XAS spectrum shown by a tick mark in the inset. Four fluorescence peaks are observed: $K\beta_{1,3}$, $K\beta'$, $K\beta''$, and $K\beta_{2,5}$. The assignment of these peaks has been explained in our previous papers.^{10,11} As was the case for the previous temperature and applied electric field dependence results, these four fluorescence peaks do not depend on d . This is simply due to the fact that the fluorescence energy is determined by the energy separation between core levels, which do not hybridize with other orbitals. Fluorescence is essentially a local process within an x-ray absorbing atom and is, therefore, not influenced by chemical bonding with ligand atoms.

Two Raman peaks due to CT excitation from O $2p$ to Ti $3d$ are observed in the range between the elastic and $K\beta_{2,5}$ peaks. This area is enlarged in Fig. 3. The vertical axis is displayed

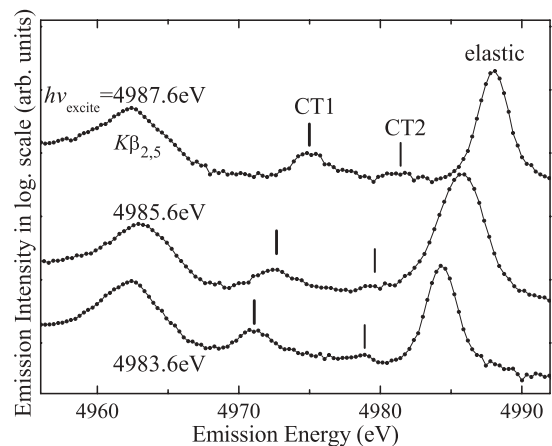


FIG. 3. Excitation x-ray energy ($h\nu_{ex}$) dependence of the Ti $K\beta$ RXES spectra around the charge transfer (CT) peaks of BTO nanoparticles with $d = 200$ nm at room temperature. The vertical axis is a logarithmic scale. $h\nu_{ex}$ is shifted by 2 eV, as evidenced by the shift in the elastic peaks.

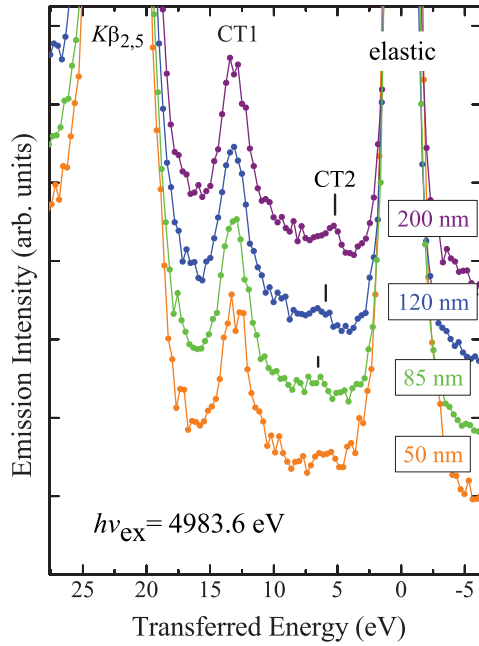


FIG. 4. (Color online) Ti $K\beta$ RXES spectra of BTO nanoparticles around the charge transfer peaks for $d = 200, 120, 85,$ and 50 nm at room temperature. The excitation x-ray energy was 4983.6 eV.

with a logarithmic scale in order to view the intense elastic peaks and weak CT peaks in one frame. With changing $h\nu_{\text{ex}}$, these two CT peaks, labeled CT1 and CT2, also change their energies, keeping the CT energies constant at $\Delta_1 = 13.5$ eV and $\Delta_2 = 5.3$ eV, respectively. This becomes evident when one notices that the $K\beta_{2,5}$ peak has a fixed energy of 4962.6 ± 0.2 eV regardless of $h\nu_{\text{ex}}$. Weak resonant features can be seen in the intensities of the CT peaks, which yield insights into the interpretation of the x-ray absorption fine structure from an electronic viewpoint.

The d -dependence of the CT peaks is shown in Fig. 4. The horizontal axis is changed to indicate transferred energy, which is the energy relative to the elastic peaks. Only four selected samples were measured because of beamtime limitations (24 h/spectrum). Similar to the fluorescence peaks, CT1 exhibits no d -dependence of its energy position or intensity. On the other hand, CT2 shows a clear d -dependence. With the decrease in d from 200 to 85 nm, CT2 shifts toward CT1 with an increase in Δ_2 from 5.3 to 6.6 eV accompanied by a gradual decrease in intensity. For $d = 50$ nm, no trace of CT2 can be found.

In previous studies, we confirmed the following two points. First, the Ti off-centering in the oxygen octahedron is a key factor affecting the CT2 energy, Δ_2 . With an increase in the Ti off-centering, i.e., enhancement of polarization, the crystallographic asymmetry between the two nonequivalent oxygen sites increases, which leads to a further difference between Δ_1 and Δ_2 . Second, the tetragonality of the unit cell is directly linked to the CT2 intensity. In the tetragonal phase, not only the difference between Δ_1 and Δ_2 but also the intensity of CT2 increases, and the opposite occurs in the cubic phase. The present results for nanoparticles follow these trends: the bulk-like 200-nm particles have a typical tetragonal structure and show a distinct CT2 peak, while the samples with smaller

particle sizes have a cubic-like structure and show a faint CT2 peak.

IV. DISCUSSION

The behavior of the CT peaks is first discussed through an energy diagram based on the CI theory. Within the framework of an ionic model, Ti has a nominal valence of $+4$ with a d^0 configuration. Under cubic or tetragonal symmetry, this $|d^0\rangle$ ground state is hybridized with $|d^1\bar{L}\rangle$ states via pd hybridization, as shown by the schematic energy diagram in Fig. 5, wherein \bar{L} denotes a ligand hole. Specifically, under spherical symmetry, the degenerate energy levels $|d^1_{t_{2g}}\bar{L}\rangle$ and $|d^1_{e_g}\bar{L}\rangle$ can be arranged into a symmetric state, $|d^1_+\bar{L}\rangle \simeq A|d^1_{t_{2g}}\bar{L}\rangle + B|d^1_{e_g}\bar{L}\rangle$, and an antisymmetric state, $|d^1_-\bar{L}\rangle \simeq B|d^1_{t_{2g}}\bar{L}\rangle - A|d^1_{e_g}\bar{L}\rangle$. The two coefficients, A and B , are comparable and have the same sign, and, in particular, are identical under spherical symmetry. The $|d^1_+\bar{L}\rangle$ state hybridizes well with the $|d^0\rangle$ state through CI interaction to form a lower-lying ground state, $|\text{GS}\rangle = c_0|d^0\rangle + c_1|d^1_+\bar{L}\rangle$, and a higher-lying CT state, $|\text{CT1}\rangle = c_1|d^0\rangle - c_0|d^1_+\bar{L}\rangle$. The energy separation between $|\text{GS}\rangle$ and $|\text{CT1}\rangle$ corresponds to Δ_1 . The $|d^1_-\bar{L}\rangle$ state is spherical-like, so that the hybridization between the spherical $|d^0\rangle$ state is quite stable. This is consistent with our results showing that the CT1 intensity and Δ_1 are insensitive to d , the temperature,¹⁰ and the electric field.¹¹

On the other hand, the hybridization between $|d^1_-\bar{L}\rangle$ and $|d^0\rangle$ is weak. Another weakly hybridized CT state, $|\text{CT2}\rangle \simeq |d^1_-\bar{L}\rangle$, is situated between $|\text{GS}\rangle$ and $|\text{CT1}\rangle$. Under cubic symmetry, the $|\text{CT2}\rangle$ state becomes faint due to the reduced hybridization. Hence, the intensity of the CT2 peak becomes fairly weak and strongly depends on the local environment around the Ti^{4+} ions. In particular, the energy position of CT2 is sensitively affected by the local Ti-O bonding, in contrast to the situation for CT1. The observed d -dependence of the CT2 peak can be understood on the basis of this energy diagram. Moreover, samples with smaller d have a larger lattice constant, as evidenced from the XRD patterns in Fig. 1(c), which further reduces the hybridization between the

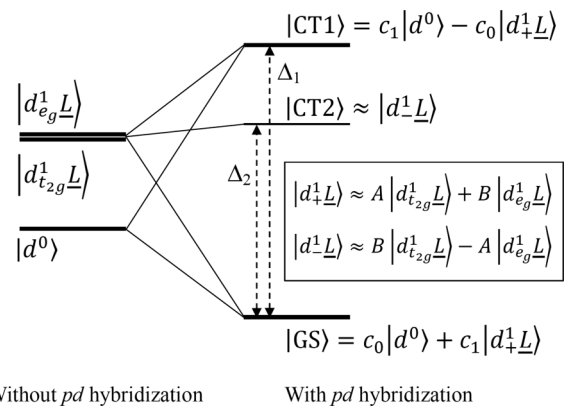


FIG. 5. Schematic energy level diagram of Ti^{4+} . Taking pd hybridization into account, the $|d^0\rangle$ ground state is hybridized with the $|d^1\bar{L}\rangle$ CT state through a configuration interaction under cubic or tetragonal symmetry. A faint CT2 state under cubic symmetry becomes clear under tetragonal symmetry.

CT states and results in the disappearance of the CT2 peak for $d = 50$ nm.

Finally, the origin of the gigantic enhancement in the dielectric constant of BTO nanoparticles at a certain size is considered from a microscopic point of view. In Ref. 4, an abrupt increase in the dielectric constant at $d = 70$ nm was reported, which was followed by a rapid decrease with decreasing d . From the XRD patterns in Fig. 1(c), the critical particle size for the transition from tetragonal to cubic is between 100 and 85 nm, while the CT2 peaks remain up to at least 85 nm and flatten out at 50 nm with decreasing particle size. The sub-100-nm particles ($d \geq 70$ nm) are in a critical phase; the crystal structure is cubic on average, whereas a Ti^{4+} ion is placed inside the local Td symmetry. That is, in a cubic oxygen octahedron, the Ti off-centering still remains. This trend can be also verified by the nonmonotonic change in FWHM of the {200} peaks for $d \leq 85$ nm. Judging from the d -dependence of CT2, the reduction of Ti off-centering with decreasing d is monotonic. At the same time, the Ti-O bonding is relaxed in an enlarged cubic cell. The Ti off-centering then becomes susceptible to the electric field, leading to enhancement of the dielectric response. The remaining off-centered Ti in the cubic phase is similar to the high-temperature NMR results⁷ and can be seen as a general property of BTO.

Recent high-precision XRD measurements provide detailed information on crystal structures together with fine electronic density distributions; however, these are averaged results. On

the other hand, the RXES technique is rather sensitive to local environments around the atom in focus and, therefore, can be a useful method for obtaining electronic information of nanosized materials.

V. CONCLUSION

We have measured the Ti $K\beta$ RXES spectra of BTO nanoparticles with various d values ranging from a bulk-like 200 nm to a paraelectric 50 nm. With decreasing d , the crystal structure changes from tetragonal to cubic, followed by a reduction in the CT2 peak intensity; i.e., the Ti off-centering remains even in the cubic phase around the critical size of $d = 85$ nm. This may be the origin of the gigantic enhancement of the dielectric constant of BTO nanoparticles. An energy diagram based on the CI model is also presented to account for the two CT peaks. These Raman peaks observed in RXES represent a sensitive probe of the local environment of absorbing atoms.

ACKNOWLEDGMENTS

We thank H. Kurokawa of TODA KOGYO Corporation for providing us with high quality samples. The staff of the Photon Factory are acknowledged for their assistance with machine operation. This work has been performed with the approval of the Photon Factory Program Advisory Committee (Proposal No. 2006G239).

*nobuo@hiroshima-u.ac.jp

¹G. H. Haertling, *J. Am. Ceram. Soc.* **82**, 797 (1999).

²K. Buse, L. Holtmann, and E. Krätzig, *Opt. Commun.* **85**, 183 (1991).

³H. Takeda, W. Aoto, and T. Shiosaki, *Appl. Phys. Lett.* **87**, 102104 (2005).

⁴S. Wada, H. Yasuno, T. Hoshina, S.-M. Nam, H. Kakemoto, and T. Tsurumi, *Jpn. J. Appl. Phys.* **42**, 6188 (2003).

⁵M. Yashima, T. Hoshina, D. Ishimura, S. Kobayashi, W. Nakamura, T. Tsurumi, and S. Wada, *J. Appl. Phys.* **98**, 014313 (2005).

⁶S. Aoyagi, Y. Kuroiwa, A. Sawada, H. Kawaji, and T. Atake, *J. Therm. Anal. Cal.* **81**, 627 (2005).

⁷B. Zalar, A. Lebar, J. Seliger, R. Blinc, V. V. Laguta, and M. Itoh, *Phys. Rev. B* **71**, 064107 (2005).

⁸R. Z. Tai, K. Namikawa, A. Sawada, M. Kishimoto, M. Tanaka, P. Lu, K. Nagashima, H. Maruyama, and M. Ando, *Phys. Rev. Lett.* **93**, 087601 (2004).

⁹K. Namikawa, M. Kishimoto, K. Nasu, E. Matsushita, R. Z. Tai, K. Sukegawa, H. Yamatani, H. Hasegawa, M. Nishikino, M. Tanaka, and K. Nagashima, *Phys. Rev. Lett.* **103**, 197401 (2009).

¹⁰Y. Isohama, N. Nakajima, H. Maruyama, Y. Tezuka, and T. Iwazumi, *J. Electron Spectrosc. Relat. Phenom.* **184**, 207 (2011).

¹¹Y. Isohama, N. Nakajima, G. Watanabe, M. Mizumaki, N. Kawamura, and H. Maruyama, *Jpn. J. Appl. Phys.* **50**, 09NE04 (2011).

¹²T. Iwazumi, K. Kobayashi, S. Kishimoto, T. Nakamura, S. Nanao, D. Ohsawa, R. Katano, and Y. Isozumi, *Phys. Rev. B* **56**, R14267 (1997).